Turkish Journal of Electrical Engineering & Computer Sciences

http://journals.tubitak.gov.tr/elektrik/

Research Article

Turk J Elec Eng & Comp Sci
(2022) 30: 2554 – 2567

doi:10.55730/1300-0632.3955

Computationally efficient predictive torque control strategies without weighting factors

Emrah ZERDALI[1,*], **Mert ALTINTAS**[1], **Ali BAKBAK**[2], **Erkan MESE**[1]
[1]Department of Electrical and Electronics Engineering, Faculty of Engineering, Ege University, Izmir, Turkey
[2]Department of Electrical and Electronics Engineering, Faculty of Engineering,
Manisa Celal Bayar University, Manisa, Turkey

Received: 06.03.2022 • **Accepted/Published Online:** 21.09.2022 • **Final Version:** 28.11.2022

Abstract: Predictive torque control (PTC) is a promising control method for electric machines due to its simplicity, fast dynamics, ability to handle nonlinearities, and easy inclusion of additional control objectives. The main challenge in conventional PTC design is to determine the weighting factors in the cost function. These weighting factors are generally chosen by the trial-and-error method or metaheuristic optimization algorithms, but these methods may not apply the optimum voltage vectors according to changing operating conditions. There are also several studies on the elimination of the weighting factors. This paper proposes two weighting factorless PTC strategies with lower computational complexities than the current literature. To demonstrate the superiority of the proposed methods, their performances are experimentally compared to those of the existing methods through a test bed equipped with an induction motor. Finally, two PTC strategies with a simple design and improved performance are introduced to the literature.

Key words: Electric motor drive, induction motor, predictive torque control, model predictive control

1. Introduction

Induction motor (IM) constitutes a crucial part of electric drive systems in the industry thanks to its ruggedness, simple structure, and low-cost. However, its highly nonlinear structure with time-varying parameters and unknown disturbances makes its control difficult. For a long time, two mature control techniques, field-oriented control (FOC) and direct torque control (DTC), have been widely applied for their high-performance control. As stated in the literature, FOC and DTC have their limitations [1–3] and more advanced control techniques are required for their high-performance control. Over the past decade, model predictive control (MPC) strategies have filled this gap, with the advantages of handling nonlinearities, easy inclusion of additional control objectives, and fast dynamic response [4].

The most attractive MPC strategy for IM control is predictive torque control (PTC) as it does not require an external modulator. PTC directly uses the discrete nature of power converters, resulting in complexity reduction. However, this superiority causes other problems: current harmonics, torque ripples, and variable switching frequency. Two effective ways to deal with these problems are to use an external modulator [5–7] and higher-level inverter topologies [7–9].

The PTC strategy combines all control objectives into a single cost function through weight factors and uses this cost function to select the optimal voltage vector for the next sampling time. The choice of these

*Correspondence: emrah.zerdali@ege.edu.tr

weighting factors is key to designing a high-performance PTC. Many researchers in the literature have focused on solving the specified design problem and different solutions have been proposed which can be divided into two main parts: studies focusing on the selection of weighting factors [8–15] and studies focusing on eliminating weighting factors [16–25].

Considering the first group of studies, various methods such as the trial-and-error method [8–10], optimization-based methods [11–14], and analytical methods [15] have been used in the selection of weighting factors. These approaches assume that the weighting factors are constant for all operating conditions, resulting in a decrease in control performance. A recent trend is the elimination of weighting factors in order to ensure a higher control performance for all operating conditions.

In the second group of studies, multiobjective ranking (MR) [16, 17], multiobjective fuzzy-decision-making (MFDM) [18], online optimization [19], sequential [20], parallel [21], predictive flux control (PFC) [22], amplitude-phase motion equation (APME) [23], technique for order of preference by similarity to ideal solution (TOPSIS) [24], and grey relational analysis (GRA) [25]-based methods have been proposed. A comparison study was conducted by Mamdouh et al. [26] between conventional, MR, MFDM, TOPSIS, and PFC. The authors state that MR has the worst performance, while MFDM, TOPSIS, and PFC have higher control performance than the conventional PTC. Furthermore, the MR method suffers from the computational complexity that increases significantly with the number of voltage vectors, objectives, and prediction horizons [16]. To overcome this problem, a hybrid sorting algorithm has been proposed in [17]. Although the MFDM method [18] provides a higher control performance, its design is complicated and requires expert knowledge. The simulated annealing-based online optimization proposed by Davari et al. [19] is not suitable for such an application due to the low convergence speed and high computational complexity of the metaheuristic algorithms. The sequential [20] and parallel [21] PTC methods provide an effective solution, but their design is getting more and more difficult with the increase in voltage vectors, objectives, and prediction horizons. The PFC method is another effective solution to eliminate the weighting factors and therefore has become the focus of interest. However, it uses weighting factors for additional control objectives [27]. A few attempts have been made in the literature for the weighting factorless PFC [28, 29]. APME [23] is based on independent control of flux and torque components as in FOC. Due to the new formulation, it needs an additional linear controller that complicates the tuning process. The last two approaches, TOPSIS [24] and GRA [25], provide a flexible design and are available to extend for an increasing number of voltage vectors, objectives, and prediction horizons with a slight computational load.

The main contribution of this paper is to design two novel weighting factorless PTC strategies based on Euclidean distance selection (EDS) and absolute distance selection (ADS). The superiority of the proposed PTC strategies over the existing methods is to have a simple mechanism and lower computational complexity. In addition, their computational complexities slightly increase in the use of higher-order inverter topologies, additional control objectives, and long prediction horizons, which are a major challenge for existing methods in practice. To clearly show their effectiveness, conventional PTCs with different weighting factors [8] and TOPSIS-based PTC [24] are also considered and their control performances are compared to those of the proposed EDS-based PTC (EDS-PTC) and ADS-based PTC (ADS-PTC) strategies.

The remainder of this paper is divided into four sections. Section 2 presents the conventional PTC strategy of IM fed by a two-level voltage source inverter (2L-VSI) and addresses the challenges. Section 3 introduces the proposed PTC strategies without weighting factors. Section 4 presents the experimental results and observations. Finally, Section 5 gives the conclusion.

2. Conventional PTC strategy

In this section, the conventional PTC strategy for IM control is presented and is evaluated in terms of the cost function and weighting factors.

2.1. IM Model Fed by 2L-VSI

The IM model in the stator stationary axis can be expressed in the following compact form:

$$\dot{\mathbf{x}}_t = \mathbf{f}(\mathbf{x}_t, \mathbf{u}_t) + \mathbf{w}_t \tag{1a}$$

$$\mathbf{z}_t = \mathbf{h}(\mathbf{x}_t) + \mathbf{v}_t \tag{1b}$$

where

$$\mathbf{x}_t = \begin{bmatrix} i_{s\alpha} & i_{s\beta} & \psi_{r\alpha} & \psi_{r\beta} & \omega_m \end{bmatrix}^T,$$

$$\mathbf{u}_t = \begin{bmatrix} v_{s\alpha} & v_{s\beta} \end{bmatrix}^T,\ \mathbf{h}(\mathbf{x}_t) = \begin{bmatrix} i_{s\alpha} & i_{s\beta} & \omega_m \end{bmatrix}^T,$$

and

$$\mathbf{f}(\mathbf{x}_t, \mathbf{u}_t) = \begin{bmatrix} -\frac{1}{T_\sigma} i_{s\alpha} + \frac{k_r}{T_r L_\sigma}\psi_{r\alpha} + \frac{k_r}{L_\sigma}\omega_r \psi_{r\beta} + \frac{v_{s\alpha}}{L_\sigma} \\ -\frac{1}{T_\sigma} i_{s\beta} + \frac{k_r}{L_\sigma T_r}\psi_{r\beta} - \frac{k_r}{L_\sigma}\omega_r \psi_{r\alpha} + \frac{v_{s\beta}}{L_\sigma} \\ \frac{L_m}{T_r} i_{s\alpha} - \frac{1}{T_r}\psi_{r\alpha} - \omega_r \psi_{r\beta} \\ \frac{L_m}{T_r} i_{s\beta} - \frac{1}{T_r}\psi_{r\beta} + \omega_r \psi_{r\alpha} \\ \frac{3}{2} k_r \frac{p_p}{J_t}(\psi_{r\alpha} i_{s\beta} - \psi_{r\beta} i_{s\alpha}) - \frac{B_t}{J_t}\omega_m - \frac{\tau_l}{J_t} \end{bmatrix}.$$

Here, $v_{s\alpha\beta}$, $i_{s\alpha\beta}$, and $\psi_{r\alpha\beta}$ are the stator stationary axis components of stator voltages, stator currents, and rotor fluxes, respectively; p_p is the pole-pairs; ω_m and ω_r $(= p_p\omega_m)$ are the mechanical and electrical angular rotor speed; τ_l is the load torque; R_s and R_r are the stator and rotor resistances, respectively; L_s and L_r are the stator and rotor inductances, respectively; L_m and L_σ $(= L_s - L_m^2/L_r)$ are the mutual and leakage inductances, respectively; B_t and J_t are the total viscous friction and inertia of both load and motor, respectively; k_r $(= L_m/L_r)$ is the rotor coupling factor; R_σ $(= R_s + k_r^2 R_r)$ is the equivalent resistance referred to the stator side; T_σ $(= L_\sigma/R_\sigma)$ is the transient time constant of stator; and T_r $(= L_r/R_r)$ is the rotor time constant.

Using first-order forward Euler approximation

$$\dot{\mathbf{x}}_t \approx \frac{\mathbf{x}_{k+1} - \mathbf{x}_k}{T}, \tag{2}$$

the discretized IM model can be obtained as follows:

$$\mathbf{x}_{k+1} = \mathbf{I}_{5\times5} \cdot \mathbf{x}_k + \mathbf{f}(\mathbf{x}_t, \mathbf{u}_t) \cdot T, \tag{3}$$

where T is the sampling time and $\mathbf{I}_{5\times5}$ is the identity matrix with the dimension of 5×5.

When a 2L-VSI in Figure 1a is applied, the inverter output voltage $\boldsymbol{v}_s$ can be expressed as:

$$\boldsymbol{v}_s = \frac{2}{3} V_{\mathrm{dc}}(S_a + aS_b + a^2 S_c), \tag{4}$$

where a is the phase shift of 120 electrical degree, $V_{\rm dc}$ is the dc-link voltage, and $S_x \in \{S_a, S_b, S_c\}$ indicates ON/OFF states of upper switches on each leg.

Seven different voltage vectors, called finite control set, can be generated by (4) for eight switching combinations. These voltage vectors are shown in Figure 1b.

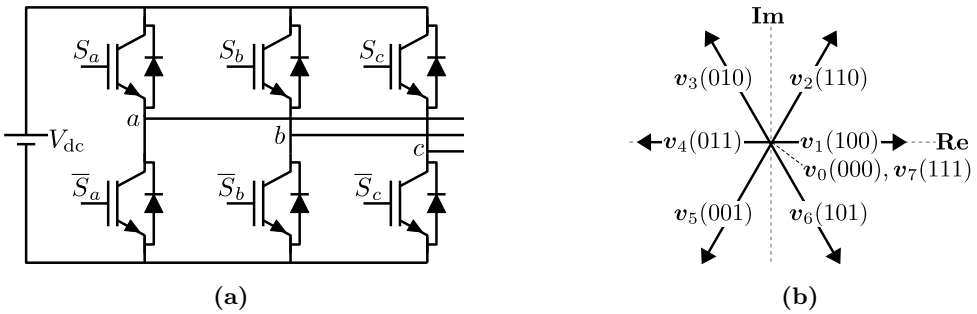

Figure 1. 2L-VSI (a) Circuit topology, (b) possible voltage vectors.

2.2. Conventional PTC strategy

The overall block diagram of the PTC-controlled IM drive is presented in Figure 2, and the PTC strategy consists of two blocks: torque/flux prediction and cost function optimization. Because PTC requires flux information, the drive system also has a flux estimation block. Considering the flux estimation block first, rotor flux can be estimated using the current model of IM given in (5).

$$\boldsymbol{\psi}^e_{r,k+1} = \boldsymbol{\psi}^e_{r,k} + T_s \left[\frac{L_m}{T_r} \boldsymbol{i}_{s,k} - \left(\frac{1}{T_r} - j\omega_{r,k} \right) \boldsymbol{\psi}^e_{r,k} \right] \tag{5}$$

Next, stator flux can be calculated using the measured stator current vector $\boldsymbol{i}_{s,k}$ $(= i_{s\alpha,k} + j i_{s\beta,k})$ and estimated rotor flux vector $\boldsymbol{\psi}^e_{r,k}$ $(= \psi^e_{r\alpha,k} + j\psi^e_{r\beta,k})$ as follows:

$$\boldsymbol{\psi}^e_{s,k} = \frac{L_m}{L_r} \boldsymbol{\psi}^e_{r,k} + L_\sigma \boldsymbol{i}_{s,k} \tag{6}$$

As for the second block, the stator flux and stator current at the time of $k+1$ can be predicted as:

$$\boldsymbol{\psi}^p_{s,k+1} = \boldsymbol{\psi}^e_{s,k} + T\boldsymbol{v}_{s,k} - TR_s \boldsymbol{i}_{s,k} \tag{7}$$

and

$$\boldsymbol{i}^p_{s,k+1} = \left(1 - \frac{T}{T_\sigma} \right) \boldsymbol{i}_{s,k} + \frac{T}{T_\sigma R_\sigma} \cdot \left(\left(\frac{k_r}{T_r} - k_r j\omega_{r,k} \right) \boldsymbol{\psi}^e_{r,k} + \boldsymbol{v}_{s,k} \right). \tag{8}$$

In real-time applications of PTC strategy, the time delay resulting from the calculation of the control algorithm has a significant effect on the control performance. For this purpose, the two-step-ahead prediction algorithm [8, 30], a well-known delay compensation method, is included in all PTC strategies. The compensated stator flux $\boldsymbol{\psi}^p_{s,k+2}$ and stator current $\boldsymbol{i}^p_{s,k+2}$ are as follows:

$$\boldsymbol{\psi}^p_{s,k+2} = \boldsymbol{\psi}^e_{s,k+1} + T\boldsymbol{v}_{s,k+1} - TR_s \boldsymbol{i}_{s,k+1} \tag{9}$$

and

$$\boldsymbol{i}^{p}_{s,k+2} = \left(1 - \frac{T}{T_\sigma}\right)\boldsymbol{i}_{s,k+1} + \frac{T}{T_\sigma R_\sigma} \cdot \left(\left(\frac{k_r}{T_r} - k_r j\omega_{r,k}\right)\boldsymbol{\psi}^{e}_{r,k+1} + \boldsymbol{v}_{s,k+1}\right). \tag{10}$$

Consequently, the electromagnetic torque can be calculated using the compensated stator flux $\boldsymbol{\psi}^{p}_{s,k+2}$ and stator current $\boldsymbol{i}^{p}_{s,k+2}$ as follows:

$$\tau^{p}_{e,k+2} = \frac{3}{2} p_p \Im m\left\{(\boldsymbol{i}^{p}_{s,k+2})(\boldsymbol{\psi}^{p}_{s,k+2})^*\right\}. \tag{11}$$

In the conventional PTC strategy, the optimum voltage vector is selected through the predefined multiobjective cost function that includes different control objectives. As in (12), there are two main control objectives that are needed to control torque and flux. Besides, additional control objectives can be included through weighting factors.

$$g = \left|\tau^{*}_{e} - \tau^{p}_{e,k+2}\right| + \lambda_\psi \left||\boldsymbol{\psi}^{*}_{s}| - |\boldsymbol{\psi}^{p}_{s,k+2}|\right|, \tag{12}$$

where λ_ψ is the weighting factor of flux error.

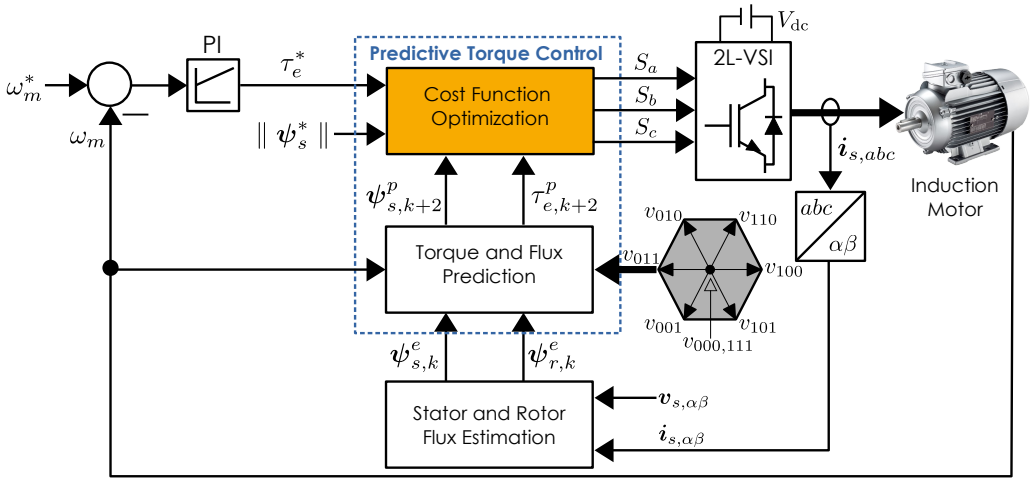

Figure 2. Block diagram of the PTC-based IM drive.

The definition of the multiobjective cost function in the conventional PTC strategy is based on the scalarization method in which all objectives are defined as weighted sums. This definition requires the determination of weighting factors and there is no analytical or systematic way in determining these factors. They are generally determined by the trial-and-error method or metaheuristic optimization methods. To overcome the mentioned difficulty, different PTC strategies without weighting factors have been proposed.

3. PTC strategies without weighting factors

In this paper, two PTC strategies without weighting factors, EDS-PTC and ADS-PTC, are proposed. Both strategies eliminate weighting factors by considering each control objective separately without using the scalarization method. The two main control objectives in the conventional PTC strategy can be defined as separate

cost functions as follows:

$$g_1 = \left| \tau_e^* - \tau_{e,k+2}^p \right|, \tag{13}$$

$$g_2 = \left| |\boldsymbol{\psi}_s^*| - |\boldsymbol{\psi}_{s,k+2}^p| \right|. \tag{14}$$

Consequently, it is possible to design different weighting factorless PTC strategies through these cost functions. The flowchart of the two proposed strategies in this paper is presented in Figure 3.

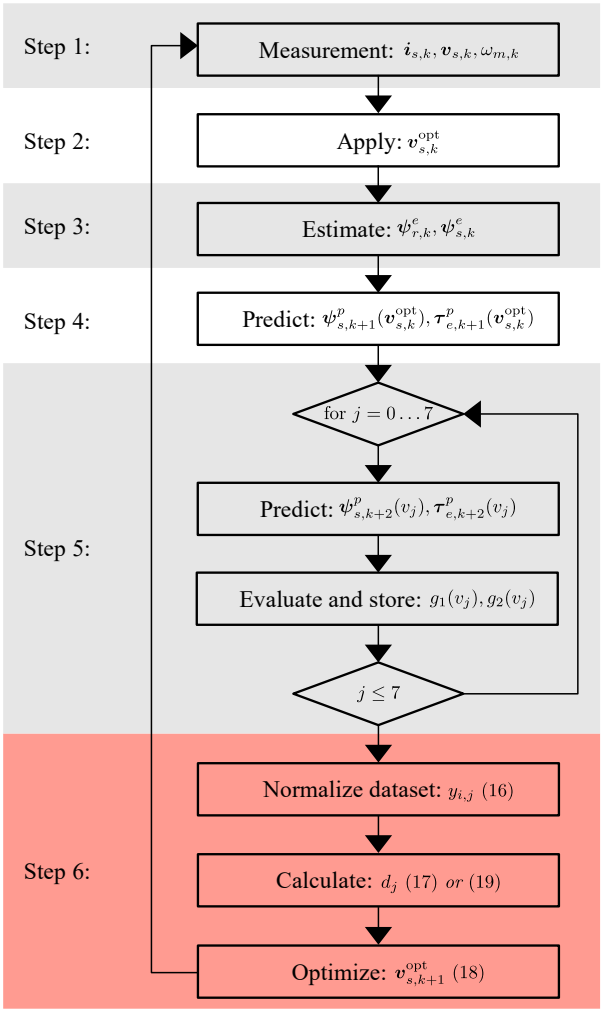

Figure 3. Flowchart of the proposed PTC strategies without weighting factors.

3.1. Euclidean distance selection-based PTC

The EDS-based strategy consists of the following steps:

1. Generation of dataset:

$$x_{ij} = \begin{pmatrix} g_1(\boldsymbol{v}_0) & g_2(\boldsymbol{v}_0) & \dots & g_n(\boldsymbol{v}_0) \\ g_1(\boldsymbol{v}_1) & g_2(\boldsymbol{v}_1) & \dots & g_n(\boldsymbol{v}_1) \\ \vdots & \vdots & \ddots & \vdots \\ g_1(\boldsymbol{v}_m) & g_2(\boldsymbol{v}_m) & \dots & g_n(\boldsymbol{v}_m) \end{pmatrix}, \tag{15}$$

where $i \in \{0, 1, \ldots, n\}$ and $j \in \{1, 2, \ldots, m\}$ indicate the number of control objectives and voltage vectors, respectively.

2. Normalization of the dataset:

$$y_{ij} = \frac{x_i^{\min} - x_{ij}}{x_i^{\min} - x_i^{\max}} \tag{16}$$

3. Next, the Euclidean distances between the origin and the set of cost values for each voltage vector are calculated (see Figure 4):

$$d_j(p_j, 0) = \sqrt{(y_{j,1})^2 + (y_{j,2})^2 + \ldots + (y_{j,n})^2} \tag{17}$$

4. Finally, the jth voltage vector that minimizes the d_j is selected:

$$\boldsymbol{v}_{\text{opt}} = \arg\min_j d_j \tag{18}$$

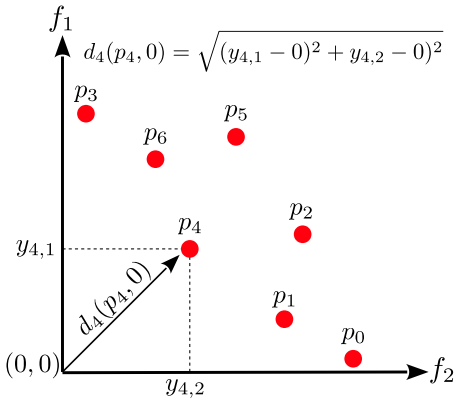

Figure 4. Representation of Euclidean distance in two-dimensional space.

3.2. Absolute distance selection-based PTC

To prevent the computational load caused by taking the square and square root in the EDS-PTC strategy, the ADS-PTC strategy is also proposed. The only difference between both methods is in the calculation of distances in (17) and the following expression is used instead of the Euclidean distance:

$$d_j(p_j, 0) = y_{j,1} + y_{j,2} + \ldots + y_{j,n} \tag{19}$$

The main advantage of EDS and ADS based strategies is that they can be extended with additional control objectives with a slight difference in computational complexity. For example, the computational complexities of multiobjective ranking, parallel, and serial-based strategies rise extremely with increasing prediction horizon, the number of cost functions, and the number of possible switching combinations. This feature makes the proposed strategies more suitable for higher-level inverter topologies and PTC strategies having additional control objectives. This case will be addressed in detail in Section 4.4.

4. Experimental results and observations

In this section, firstly, the features of the testbed are introduced and then real-time experiments are presented. Execution times for all strategies are also given to compare computational complexities. Finally, observations are presented.

4.1. Experimental setup

Experimental tests have been carried out in the testbed shown in Figure 5. This setup consists of a three-phase squirrel-cage IM, a Foucault brake as load machine, and a motor drive unit. The rated values and parameters of three-phase IM used in experimental studies are given in Table 1. A lab-made motor drive unit is used in which phase currents and dc-link voltage are measured by LEM CAS 6-NP current transducers and a lab-made voltage transducer, respectively. A 1024 p/r encoder is used for speed measurement. All PTC strategies are implemented on an STM32F407VGT6 microcontroller featuring 32-bit Arm Cortex®-M4 with FPU core.

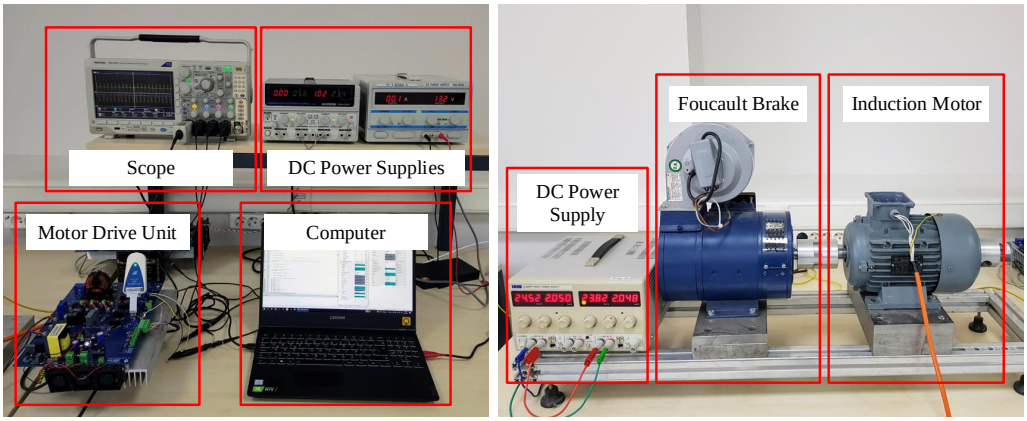

Figure 5. Experimental setup.

Table 1. The rated values and parameters of the IM.

Parameter	Value	Parameter	Value
P	1.5 kW	p_p	2
V	380 V	R_s	5.22 Ω
I	3.7 A	R_r	3.67 Ω
f	50 Hz	L_m	0.2478 H
n_m	1390 r/min	L_s	0.01363 H
τ_l	10 Nm	L_r	0.01363 H

4.2. Experimental results

This section firstly shows the effect of different weighting factors on traditional PTC performance. For this purpose, conventional PTCs with weighting factors of 20, 30, and 40 are considered. Subsequently, experimental results are presented for TOPSIS-PTC, EDS-PTC, and ADS-PTC, respectively, to confirm the effectiveness of the proposed methods. In the implementation of TOPSIS-PTC, the weighting factors for torque and stator flux are used as 0.5, so both are of equal importance. The sampling frequency for all control methods is 16 kHz and a PI-type speed controller with the same gains is used in all tests.

The performance of conventional PTCs with different weighting factors is studied under load variations of 6 Nm at 750 r/min. Considering the control performances in Figure 6, there is a nonlinear relationship between the weighting factor and control performance. An increase in the value of the weighting factor results in a significant reduction in flux fluctuations. Because the flux error term has a higher effect on the cost function. Besides, lower flux fluctuations also lead to reduction in torque fluctuations. Contrary to this effect, the increasing effect of the flux error term in the cost function degrades the torque control performance. For this reason, a detailed analysis should be made to obtain the optimum weighting factor, taking into account the changing operating conditions. On the other hand, there is no significant difference in speed control performance for the given scenario. However, the assumption of fixed weighting factors in conventional PTC strategies causes degradation in their control performances due to the changing optimal weighting factors according to operating conditions. To deal with this problem, the weighting factors should be updated online or eliminated to achieve higher control performance.

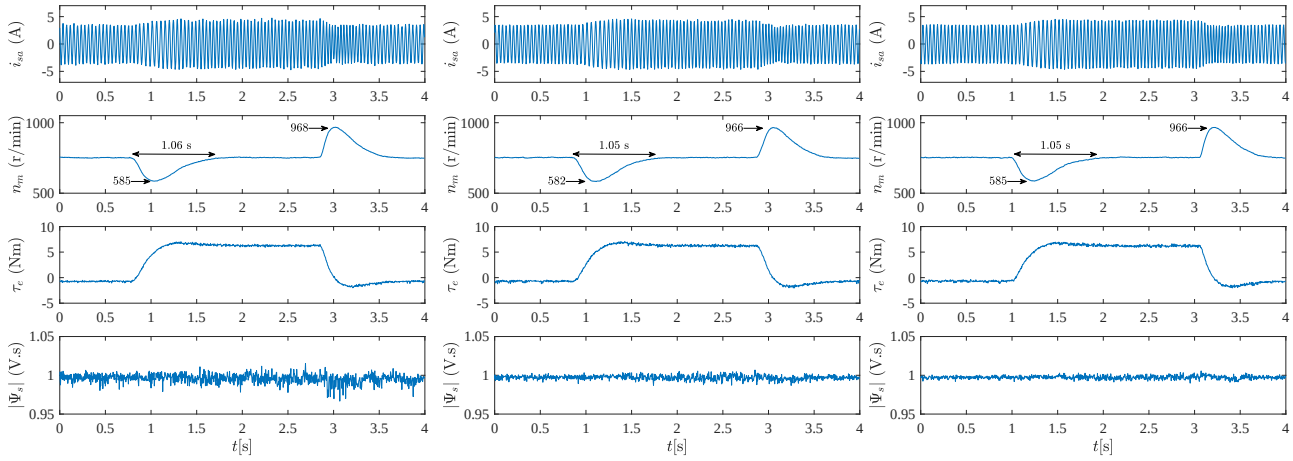

Figure 6. Experimental results: Control performance of conventional PTC strategies under load changes at 750 r/min (a) PTC with $\lambda_\psi = 20$, (b) PTC with $\lambda_\psi = 30$, (c) PTC with $\lambda_\psi = 40$.

In testing of TOPSIS-PTC, EDS-PTC, and ADS-PTC strategies, two different tests are performed in which load change and speed changes are made. In the first test, all PTCs without weighting factors are tested under load changes of 6 Nm at 750 r/min, similar to the test for conventional PTCs with different weighting factors. In the second test, their performance is examined for a speed reversal from +1000 r/min to −1000 r/min under a 6.5 Nm load.

The results for the first test presented in Figure 7 demonstrate that TOPSIS-PTC has similar speed control performance (see Figure 7a) to conventional PTC but provides lower flux fluctuations for different operating conditions than conventional PTC with a poorly tuned weighting factor. Compared to previous strategies, both EDS-PTC and ADS-PTC provide better speed control performance (see Figures 7b and 7c) with reduced overshoot and settling time despite using the same speed controller in all tests. It is clear that among the EDS-PTC and ADS-PTC strategies, the best control performance belongs to EDS-PTC.

The results for the second test in Figure 8 demonstrate that control performance can be improved using weighting factorless design strategies in all operating conditions. In addition, the proposed weighting factorless PTC strategies, EDS-PTC and ADS-PTC, have superior control performance in terms of dynamic response and

torque control over the TOPSIS-PTC proposed in [24].

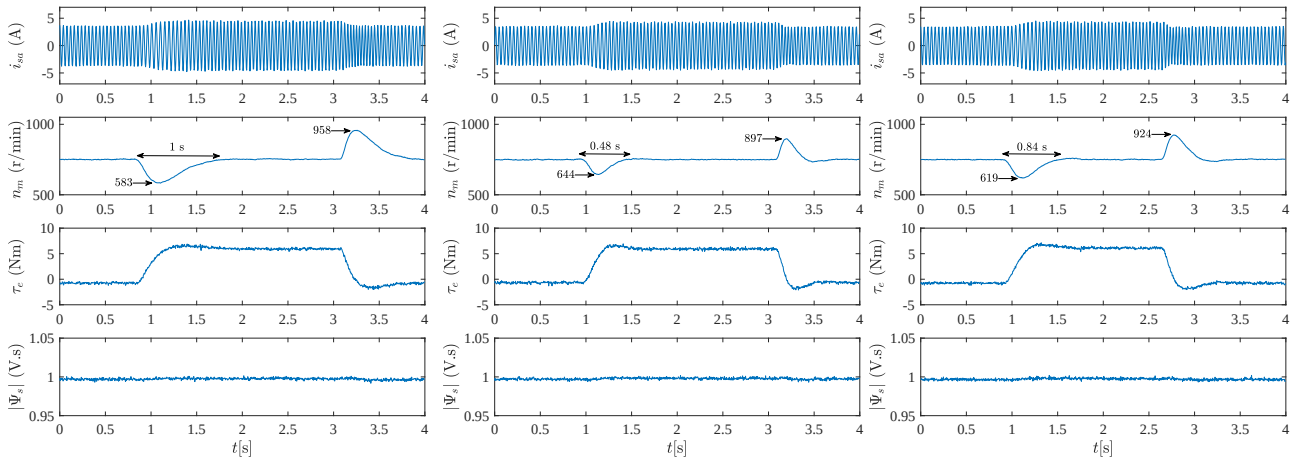

Figure 7. Experimental results: Control performance of weighting factorless PTC strategies under load changes of 6 Nm at 750 r/min (a) TOPSIS-PTC in [24], (b) EDS-PTC, (c) ADS-PTC.

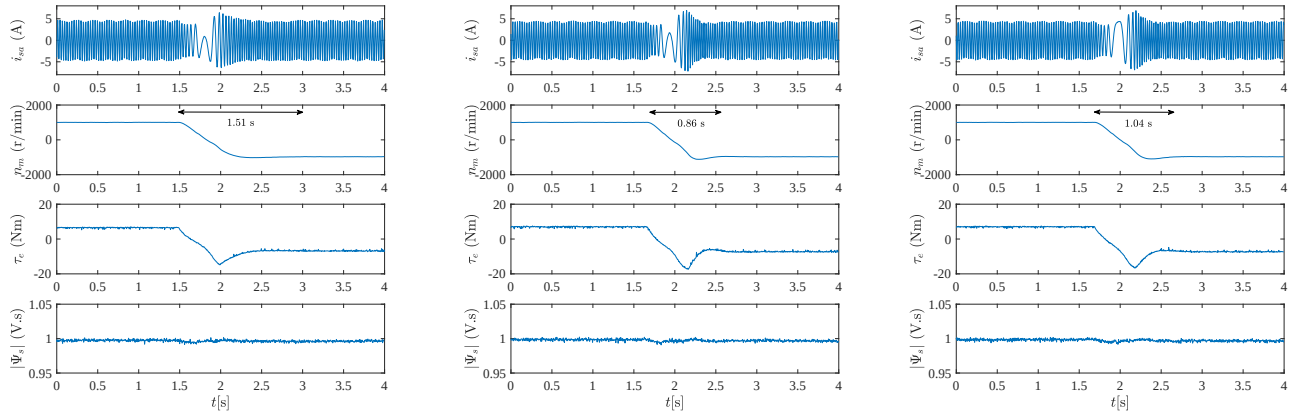

Figure 8. Experimental results: Control performance of weighting factorless PTC strategies for a speed reversal from +1000 r/min to −1000 r/min under a load of 6.5 Nm. (a) TOPSIS-PTC in [24] (b) EDS-PTC (c) ADS-PTC

To quantitatively support the results in Figures 7 and 8, flux ripples (ψ_{rip}), torque ripples (τ_{rip}), total harmonic distortions (THDs) of stator currents (i_{THD}), and average switching frequencies (f_{avg}) at 750 r/min and 1000 r/min are presented in Figure 9, respectively. These statistics are calculated as follows:

$$\%x_{\text{rip}} = \frac{x_{\text{max}} - x_{\text{mean}}}{x_{\text{rated}}} \times 100, \tag{20}$$

where x is a dummy variable that corresponds to flux or torque and x_{max}, x_{mean}, and x_{rated} denote its

maximum value, mean value, and rated value, respectively.

$$i_{\mathrm{THD}} = 100 \times \sqrt{\left(\frac{I_{\mathrm{rms}}}{I_{1\mathrm{rms}}}\right)^2 - 1}, \tag{21}$$

where I_{rms} and $I_{1\mathrm{rms}}$ are root mean square values for phase current and its fundamental component, respectively.

$$f_{\mathrm{avg}} = \frac{N}{n_{sw} \times d}, \tag{22}$$

where N is the total changes in switching states during a time interval of d seconds. n_{sw} is the number of switches in a power converter and equals six for a 2L-VSI.

Given the overall control performance in Figure 9, flux and torque ripples can be reduced using EDS-PTC and ADS-PTC strategies with a slight increase in average switching frequency. In addition to improvement in control performance at 750 r/min, it is also possible to reduce the THD of stator current with the proposed weighting factorless PTC strategies.

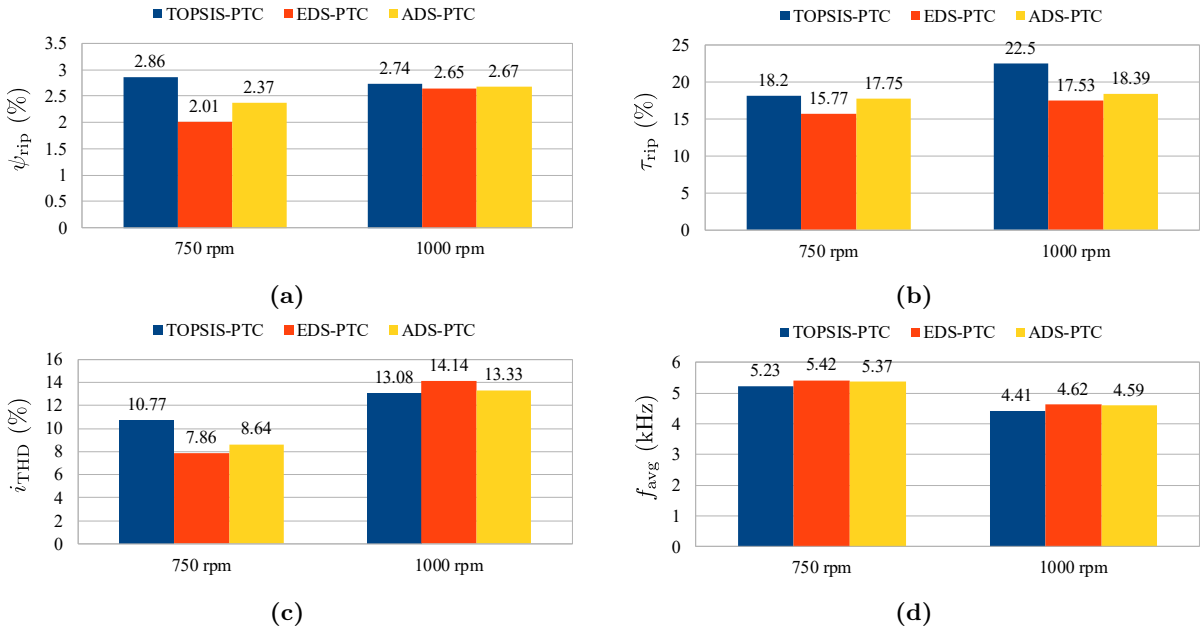

Figure 9. Results at 750 r/min under 6 Nm load and 1000 r/min under 6.5 Nm load (a) ψ_{rip} (%), (b) τ_{rip} (%), (c) i_{THD} (%), (d) f_{avg}.

4.3. Computational complexity

So far, PTC strategies without weighting factors have been compared considering only their control performances, but another important consideration in practice is computational complexity. Therefore, a method should be chosen considering the trade-off between control performance and computational complexity. To this end, the measured execution times of the three weighting factorless PTC strategies are given in Table 2 to compare computational complexities. It is clear that the PTC strategies without weighting factors increase the computational burden. However, both EDS-PTC and ADS-PTC strategies reduce the computational burden

compared to TOPSIS-PTC. The ADS-PTC strategy, created by eliminating the square root calculation in the EDS-PTC strategy, reduces the computational load by about 10%.

Table 2. Execution times for TOPSIS-PTC, EDS-PTC, and ADS-PTC.

TOPSIS-PTC	EDS-PTC	ADS-PTC
34.8 μs	28.5 μs	25.8 μs

4.4. Observations

Compared to the MR-PTC strategy [16, 17], both EDS-PTC and ADS-PTC do not need a ranking algorithm that excessively raises the computational load with increasing prediction horizon and additional control objectives. Moreover, both methods eliminate the difficulty in selecting candidate voltage vectors in sequential [20] and parallel [21] PTC strategies in case of additional control objectives. Considering all these advantages, it is possible to extend them with a slight increase in computational load. Indeed, both PTC strategies are advanced versions of TOPSIS-PTC [24] with improved control performance and reduced computational complexity. Despite the additional computational loads caused by the proposed weighting factorless designs, both PTC strategies clearly improve control performance, especially in transients.

5. Conclusion

The two weighting factorless PTC strategies proposed in this paper eliminate the problem of determining weighting factors in conventional PTCs and offer an effective and flexible solution. Experimental results demonstrate that both have better control performance than the conventional PTC strategy. Compared to the existing PTC strategies without weighting factors, they have a straightforward structure and can be easily extended with a slight increase in computational load for higher-level inverter topologies, additional control objectives, and long prediction horizons. Future studies will focus on comprehensively evaluating these PTC strategies in the presence of additional control objectives.

References

[1] Rodriguez J, Kennel RM, Espinoza JR, Trincado M, Silva CA et al. High-Performance Control Strategies for Electrical Drives: An Experimental Assessment. IEEE Transactions on Industrial Electronics 2012; 59 (2): 812-820. https://doi.org/10.1109/TIE.2011.2158778

[2] Davari SA, Khaburi DA, Wang F, Kennel R. Robust sensorless predictive control of induction motors with sliding mode voltage model observer. Turkish Journal of Electrical Engineering & Computer Sciences 2013; 21 (6): 1539-1552. https://doi.org/10.3906/elk-1110-3

[3] Korkmaz F. Performance improvement of induction motor drives with model-based predictive torque control. Turkish Journal of Electrical Engineering & Computer Sciences 2020; 28 (1): 525-539. https://doi.org/10.3906/elk-1804-124

[4] Wang F, Zhang Z, Mei X, Rodríguez J, Kennel R. Advanced Control Strategies of Induction Machine: Field Oriented Control, Direct Torque Control and Model Predictive Control. Energies 2018; 11 (1): 120. https://doi.org/10.3390/en11010120

[5] Amiri M, Milimonfared J, Khaburi DA. Predictive Torque Control Implementation for Induction Motors Based on Discrete Space Vector Modulation. IEEE Transactions on Industrial Electronics 2018: 65 (9); 6881-6889. https://doi.org/10.1109/TIE.2018.2795589

[6] Osman I, Xiao D, Alam KS, Shakib SMSI, Akter MP et al. Discrete Space Vector Modulation-Based Model Predictive Torque Control With No Suboptimization. IEEE Transactions on Industrial Electronics 2019; 67 (10): 8164-8174. https://doi.org/10.1109/tie.2019.2946559

[7] Wang Q, Yu H, Li C, Lang X, Yeoh SS et al. A Low-Complexity Optimal Switching Time-Modulated Model-Predictive Control for PMSM With Three-Level NPC Converter. IEEE Transactions on Transportation Electrification 2020; 6 (3): 1188-1198. https://doi.org/10.1109/TTE.2020.3012352

[8] Habibullah M, Lu DDC, Xiao D, Fletcher JE, Rahman MF. Predictive Torque Control of Induction Motor Sensorless Drive Fed by a 3L-NPC Inverter. IEEE Transactions on Industrial Informatics 2017; 13 (1): 60-70. https://doi.org/10.1109/TII.2016.2603922

[9] Lakhimsetty S, Somasekhar VT. An Efficient Predictive Current Control Strategy for a Four-Level Open-End Winding Induction Motor Drive. IEEE Transactions on Power Electronics 2020; 35 (6): 6198-6207. https://doi.org/10.1109/TPEL.2019.2954864

[10] Zerdali E, Demir R. Speed-sensorless predictive torque controlled induction motor drive with feed-forward control of load torque for electric vehicle applications. Turkish Journal of Electrical Engineering & Computer Sciences 2021; 29 (1): 223-240. https://doi.org/10.3906/elk-2005-75

[11] Ahmed AA, Koh BK, Park HS, Lee KB, Lee YI. Finite-Control Set Model Predictive Control Method for Torque Control of Induction Motors Using a State Tracking Cost Index. IEEE Transactions on Industrial Electronics 2017; 64 (3): 1916-1928. https://doi.org/10.1109/TIE.2016.2631456

[12] Guazzelli PRU, de Andrade Pereira WC, de Oliveira CMR, de Castro AG, de Aguiar ML. Weighting Factors Optimization of Predictive Torque Control of Induction Motor by Multiobjective Genetic Algorithm. IEEE Transactions on Power Electronics 2018; 34 (7): 6628-6638. https://doi.org/10.1109/tpel.2018.2834304

[13] Arshad MH, Abido MA, Salem A, Elsayed AH. Weighting Factors Optimization of Model Predictive Torque Control of Induction Motor Using NSGA-II with TOPSIS Decision Making. IEEE Access 2019; 7: 177595-177606. https://doi.org/10.1109/ACCESS.2019.2958415

[14] Gurel A, Zerdali E. The Effect of Different Decision-Making Methods on Multi-Objective Optimisation of Predictive Torque Control Strategy. Power Electronics and Drives 2021; 6 (1): 289-300. https://doi.org/10.2478/pead-2021-0018

[15] Geyer T. Algebraic Tuning Guidelines for Model Predictive Torque and Flux Control. IEEE Transactions on Industrial Applications 2018; 54 (5): 4464-4475. https://doi.org/10.1109/TIA.2018.2835375

[16] Rojas CA, Rodriguez J, Villarroel F, Espinoza JR, Silva CA et al. Predictive torque and flux control without weighting factors. IEEE Transactions on Industrial Electronics 2013; 60 (2): 681-690. https://doi.org/10.1109/TIE.2012.2206344

[17] Bandy K, Stumpf P. Model Predictive Torque Control for Multilevel Inverter fed Induction Machines Using Sorting Networks. IEEE Access 2021; 9: 13800-13813. https://doi.org/10.1109/ACCESS.2021.3052129

[18] Rojas CA, Rodriguez JR, Kouro S, Villarroel F. Multiobjective Fuzzy-Decision-Making Predictive Torque Control for an Induction Motor Drive. IEEE Transactions on Power Electronics 2017; 32 (8): 6245-6260. https://doi.org/10.1109/TPEL.2016.2619378

[19] Davari SA, Nekoukar V, Garcia C, Rodriguez J. Online Weighting Factor Optimization by Simplified Simulated Annealing for Finite Set Predictive Control. IEEE Transactions on Industrial Informatics 2021; 17 (1): 31-40. https://doi.org/10.1109/TII.2020.2981039

[20] Davari SA, Norambuena M, Nekoukar V, Garcia C, Rodriguez J. Even-Handed Sequential Predictive Torque and Flux Control. IEEE Transactions on Industrial Electronics 2020; 67 (9): 7334-7342. https://doi.org/10.1109/TIE.2019.2945274

[21] Wang F, Xie H, Chen Q, Davari SA, Rodriguez J et al. Parallel Predictive Torque Control for Induction Machines Without Weighting Factors. IEEE Transactions on Power Electronics 2020; 35 (2): 1779-1788. https://doi.org/10.1109/TPEL.2019.2922312

[22] Zhang Y, Yang H, Xia B. Model-Predictive Control of Induction Motor Drives: Torque Control Versus Flux Control. IEEE Transactions on Industrial Applications 2016; 52 (5): 4050-4060. https://doi.org/10.1109/TIA.2016.2582796

[23] Lu Z, Zhang R, Hu L, Gan L, Lin J et al. Model predictive control of induction motor based on amplitude-phase motion equation. IET Power Electronics 2019; 12 (9): 2400-2406. https://doi.org/10.1049/iet-pel.2019.0093

[24] Muddineni VP, Sandepudi SR, Bonala AK. Finite control set predictive torque control for induction motor drive with simplified weighting factor selection using TOPSIS method. IET Electric Power Applications 2017; 11 (5): 749-760. https://doi.org/10.1049/iet-epa.2016.0503

[25] Muddineni VP, Bonala AK, Sandepudi SR. Grey Relational Analysis-Based Objective Function Optimization for Predictive Torque Control of Induction Machine. IEEE Transactions on Industrial Applications 2021; 57 (1): 835-844. https://doi.org/10.1109/TIA.2020.3037875

[26] Mamdouh M, Abido MA, Hamouz Z. Weighting Factor Selection Techniques for Predictive Torque Control of Induction Motor Drives: A Comparison Study. Arabian Journal for Science and Engineering 2018; 43 (2): 433-445. https://doi.org/10.1007/s13369-017-2842-2

[27] Osman I, Xiao D, Rahman MF, Norambuena M, Rodriguez J. An Optimal Reduced-Control-Set Model Predictive Flux Control for 3L-NPC Fed Induction Motor Drive. IEEE Transactions on Energy Conversion 2021; 36 (4): 2967-2976. https://doi.org/10.1109/TEC.2021.3065373

[28] Xiao D, Alam KS, Osman I, Akter MP, Shakib SMSI et al. Low Complexity Model Predictive Flux Control for Three-Level Neutral-Point Clamped Inverter-Fed Induction Motor Drives Without Weighting Factor. IEEE Transactions on Industrial Applications 2020; 56 (6): 6496-6506. https://doi.org/10.1109/TIA.2020.3016617

[29] Xiao D, Akter MP, Alam K, Dutta R, Mekhilef S et al. Cascaded Predictive Flux Control for a 3-L Active NPC Fed im Drives without Weighting Factor. IEEE Transactions on Energy Conversion 2021; 36 (3): 1797-1807. https://doi.org/10.1109/TEC.2021.3065648

[30] Cortes P, Rodriguez J, Silva C, Flores A. Delay Compensation in Model Predictive Current Control of a Three-Phase Inverter. IEEE Transactions on Industrial Electronics 2012; 59 (2): 1323-1325. https://doi.org/10.1109/TIE.2011.2157284